第 49 卷 第 7 期/2022 年 4 月/中国激光 研究论文

中国激光

用于里德堡原子激发的激光系统实现

靳刚[1*]，成永杰[1]，黄承祖[1]，刘星汛[1]，齐万泉[1]，何军[2,3]

[1]北京无线电计量测试研究所，北京 100039；

[2]山西大学光电研究所，量子光学与光量子器件国家重点实验室，山西 太原 030006；

[3]山西大学，省部共建极端光学协同创新中心，山西 太原 030006

摘要 里德堡原子具有较大的电偶极矩，可以作为一种对微波场强具有高灵敏度的传感器。制备铯里德堡原子需要 852 nm 和 509 nm 单频窄线宽可调谐激光系统，目前的 509 nm 激光系统多为实验室用样机，稳定性和实用性较差。本文提出了一种结构稳定的猫眼式激光系统，该系统可实现 200 mW，1018 nm 和 50 mW，852 nm 单频激光输出，采用电流、压电调节方式实现激光波长调谐和频率锁定；将 1018 nm 激光作为种子源，激光经过窄线宽掺镱光纤放大器后将功率放大至 5 W，之后进入光纤耦合式单通掺氧化镁周期极化铌酸锂（MgO∶PPLN）晶体进行倍频，实现了大于 470 mW 的 509 nm 激光输出。基于此激光系统实现了 $n=67$ 的里德堡原子制备，得到了线宽约为 5 MHz 的 D 态电磁诱导透明光谱，为后续构建量子微波场强测量装置提供了核心单元。

关键词 激光光学；里德堡原子；电磁诱导透明；激光系统；微波电场

中图分类号 O436 **文献标志码** A **doi**：10.3788/CJL202249.0701003

1 引 言

微波场强测量在微波通信、遥感、天线校准[1-2]等方面具有重要意义。为了突破传统微波场强测量的局限性，量子场强方案采用玻璃气室原子体系来避免使用金属天线时引入的测量误差。原子作为传感器，在物理量测量的复现性、精确度和稳定性等方面具有较大优势，目前其已在时间计量的原子钟上实现了 10^{14} 的精度[3]，在磁场探测上达到了 $\mathrm{fT}/\sqrt{\mathrm{Hz}}$ 的灵敏度[4-7]。碱原子的里德堡态能级寿命约为微秒量级，相对较长，便于实现基态和里德堡态的相干叠加态。里德堡态之间的偶极跃迁[8-10]可覆盖 1～500 GHz 的微波频率，该频率范围对应的电偶极矩是基态原子光学激发跃迁偶极矩的上千倍。利用里德堡原子较大的极化率和电偶极矩，量子场强测量可以实现更高的探测灵敏度[11-13]，测量灵敏度可达 55 $\mathrm{nV}/(\mathrm{cm}\cdot\sqrt{\mathrm{Hz}})$，最小可探测微波场强约为 400 pV/cm。基于里德堡原子的上述特征，电磁感应透明（EIT）Autler-Townes（AT）分裂方案可以实现弱场测量[12, 14-16]，而且该方案具有较高的测量准确度；AC stark 效应[17]方案可以实现宽频带的微波测量；采用原子和射频场的非线性相互作用可以实现强场的测量[18-19]。

里德堡原子制备方案包括单光子激发[20]、双光子激发[21]和三光子激发[22]。其中：单光子激发可单步激发基态原子使其跃迁到里德堡 P 态，但要求激发光子大多处于紫光和紫外光波段，光源的获取比较复杂，而且跃迁强度较小。双光子激发（如铯原子采用 852 nm 和 509 nm 双光子激发）可以实现里德堡态制备，而且 509 nm 激光的百毫瓦量级功率相对容易实现；此方案可制备 D 态或者 S 态，对应的微波可以耦合的里德堡能级选择数目较多，是目前的主流方案。三光子激发可以实现更窄的 EIT 线宽，但同样需要较大的激光功率；该方案对应的能级跃迁强度小，而且会额外带来复杂的光源系统和激发光路构型。

目前，获得波长小于 532 nm 的单频绿光激光系统通常有两种方案：1）采用种子激光器外加放大器

收稿日期：2021-07-28；**修回日期**：2021-08-29；**录用日期**：2021-09-16

通信作者：*jingang142907@163.com

(MOPA)通过晶体倍频的方式获得;2) 直接采用 509 nm 半导体激光器实现[23-25]。在第一种方案中,种子激光器可以选用半导体激光器或者光纤激光器,其中:光纤激光器通过改变光栅温度仅可实现大约 0.5 nm 的波长调谐范围,难以大范围覆盖不同主量子数的里德堡能级(几纳米量级);外腔反馈的半导体激光器(ECDL)可以实现大范围的波长调谐,微调外腔光栅即可大范围改变激光的中心波长,但波长调节程序比较繁琐且容易跳模,还会改变激光的输出角度,导致后续光路发生变化。第二种方案直接采用绿光半导体二极管,并采用光栅外腔反馈技术,可以实现 509 nm 附近激光线宽压窄,输出激光功率可达 80 mW[25]。此外,有人提出了采用 509 nm 半导体激光器外加半导体锥形放大器(TA)进行激光放大的方案,但其放大功率有限,而且输出光斑的质量较差。

近几年新发展起来的猫眼式半导体激光器[26]具有较低的成本和较高的稳定性,可用于原子钟系统[27]、法拉第反常色散光学滤波器[28]等激光光谱或原子操控实验系统的光源。本实验采用猫眼式半导体激光器作为种子光光源,其独特的猫眼构型使其可以大范围调谐波长而不影响输出激光的光路指向,便于光纤耦合进入光纤放大器,实现种子光激光的放大。相较于半导体放大技术,该技术方案可以获得高功率、高光束质量的单频激光。该方案通过单次穿过非线性晶体[29-31]实现激光倍频转换,具有结构稳定、低成本、便于实现、免调试维护等优势。此外,有人采用四镜环形腔实现激光倍频[32],该方案虽然也可以获得较高的非线性转化效率,但种子激光波长快速扫描时,腔倍频难以同步跟随,而且还需要辅助使用较多器件和设备进行锁腔,结构的机械稳定性较差。

2　系统装置

铯原子里德堡态的激发光系统包括两套单频窄线宽激光器,其波长分别为 852 nm 和 509 nm,分别对应铯原子的激发能级 $6S_{1/2}\rightarrow 6P_{3/2}$ 和 $6P_{3/2}\rightarrow nS_{1/2}$ ($D_{3/2}$,$D_{5/2}$),如图 1 所示,即采用两步激发可以实现基态和里德堡态的相干态制备。实验装置如图 2 所

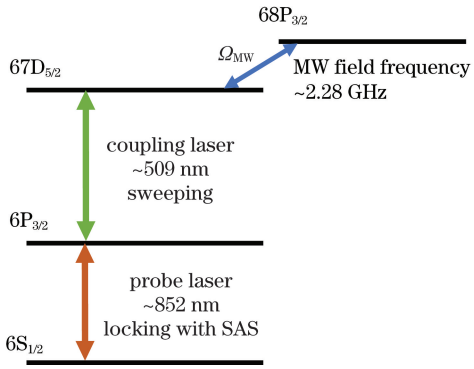

图 1　铯原子里德堡能级示意图

Fig. 1　Energy level diagram of cesium atom

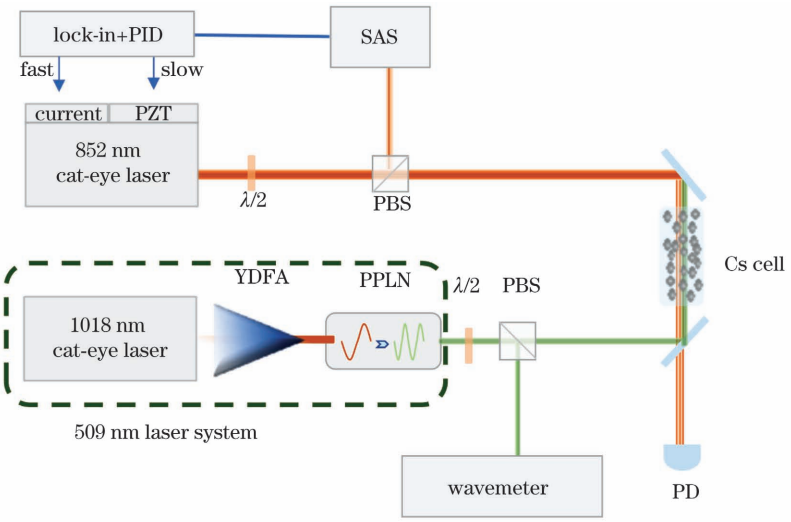

图 2　基于里德堡态的 EIT 系统示意图(λ/2 为二分之一波片,PBS 为偏振分束棱镜,SAS 为铯原子饱和吸收谱,lock-in + PID 为锁相低通和 PID 组合系统,current 为激光二极管的电流驱动端,PZT 为压电陶瓷,YDFA 为掺镱光纤放大器,PPLN 为周期极化倍频晶体,wavemeter 为 Highfiness WS-7 波长计,PD 为光电探测器)

Fig. 2　Schematic of Rydberg atom EIT setup (λ/2 represents half-wave plate, PBS represents polarizing beam splitter, SAS represents staturated absorption spectrum, lock-in +PID represents lock-in and PID module; current represents the drive current port of laser; PZT represents piezoceramics; YDFA represents ytterbium-doped fiber amplifier, PPLN represents periodically poled lithium niobate, wavemeter represents Highfiness WS-7 wavelength meter, PD represents photodetector)

示，实验中采用的是 1018 nm 和 852 nm 猫眼式外腔半导体激光器，该激光器可以实现窄线宽、高稳定性的单频激光输出，在保证激光波长大范围调谐的同时不改变激光器内部的光路方向，实现光纤耦合激光复杂链路波长的在线调谐。采用单模保偏光纤将 1018 nm 种子光耦合进单频掺镱光纤放大器（YDFA）中，YDFA 将 110 mW 种子激光放大至 5 W 输出。YDFA 后直接熔接带光纤耦合的周期极化铌酸锂（MgO∶PPLN）晶体，基频光单次通过晶体后从后端光纤输出，得到大于 470 mW 的 509 nm 倍频激光。

图 2 中的 1018 nm 和 852 nm 激光器采用猫眼式半导体结构，其结构示意图如图 3 所示。此结构的特点如下：1）具有较强的力学结构稳定性；2）波长调谐能力强，具有 PZT 外腔线性扫描调谐、电流调谐和温度慢速调谐激光波长的能力，波长调谐范围与干涉滤光片的带宽、半导体芯片的增益区间有关；3）大范围波长调谐时不改变激光的输出指向。

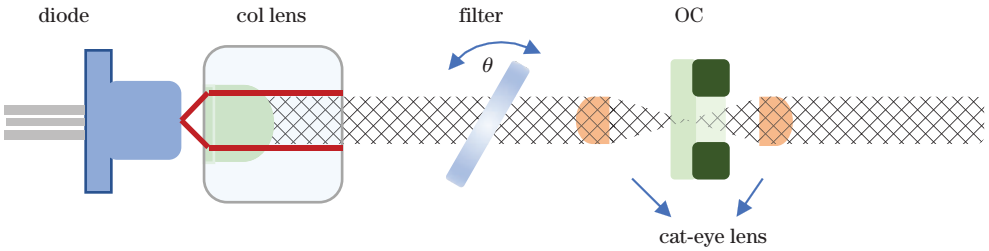

图 3　猫眼式结构激光器示意图（diode 为激光二极管；col lens 为准直透镜；filter 为窄带干涉滤光片，通过微调角度可以实现激光波长的调节；OC 为输出耦合镜）

Fig. 3　Schematic of cat-eye configure laser setup (diode represents laser emitter; col lens represents collimating lens; filter represents a narrow bandwidth filter, the emission beam wavelength can be changed via rotating the filter angle θ; OC represents the output plate)

852 nm 激光器二极管采用镀有减反膜的 GaAs 脊形波导管（EYP-RWE-0860），其类型为半导体激光管（eagleyard TO 罐型封装，内腔长 1500 μm），中心波长可调节至 852.356 nm，阈值电流为 45 mA，典型输出功率为 100 mW（电流为 180 mA 时）。隔离器型号为 MFS-835-04065，隔离度为 40 dB，透射率约为 90%。激光经过隔离器之后再经过焦距 $f=6.2$ mm 的耦合透镜进入单模保偏光纤，耦合效率为 60%。激光波长的电流调谐能力典型值为 3 MHz/μA，温度调谐能力典型值为 30 GHz/℃。

为了保证激光频率稳定，通常将激光频率锁定到原子谱线上。852 nm 激光器采用饱和吸收谱实现频率锁定，室温下其在铯原子 D2 线附近扫描可以得到饱和吸收光谱，该光谱信号经过驱动电流加弱的 250 kHz 正弦调制解调可以得到误差信号，如图 4 所示。采用 PID 组件将误差信号负反馈至压电陶瓷或者电流端口，就可以实现激光频率的稳定控制。

1018 nm 激光器二极管采用曲线增益介质芯片（GC-1030-160-TO-200-B），其中心波长可调节至 1018 nm，阈值电流为 56 mA，典型输出功率为 180～200 mW（电流为 400 mA 时）。隔离器型号为 MFD-1020-03465，隔离度为 61 dB，透射率约为 92%。激光经过隔离器之后再经过焦距 $f=4.5$ mm 耦合

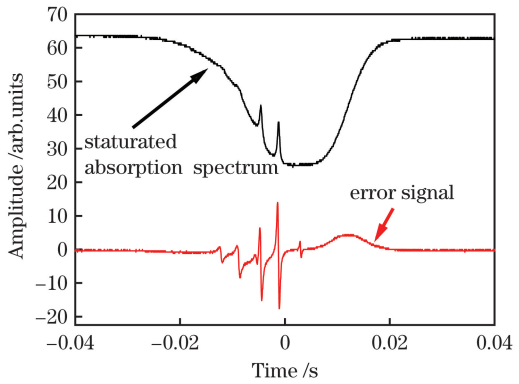

图 4　852 nm 激光器的饱和吸收光谱信号及其调制解调之后的误差信号

Fig. 4　Saturated absorption spectrum (SAS) signal of 852 nm laser and error signal after demodulating SAS signal

透镜进入单模保偏光纤，耦合效率为 64%。激光波长的电流调谐能力典型值为 3 MHz/μA，温度调谐能力典型值为 30 GHz/℃。

光纤放大器采用工作于 1 μm 波段的掺镱光纤，该光纤放大器具有效率高、稳定性好、输出光斑质量良好、便于集成化、制作简易等优点。随着商用光纤器件的成熟，此方案具有极大潜力，用于窄线宽的 1018 nm 激光放大时可以实现 5 W 量级的稳定工作。

1018 nm 激光通过光纤放大之后进入 MgO∶PPLN 实现单通晶体倍频，最大可输出 470 mW 的 509 nm 激光。相比于谐振腔倍频结构，激光单

次穿过晶体倍频[31, 33-34]后，在线宽、噪声、连续频率调谐方面具有显著优势。同时，采用晶体倍频可以避免使用锁腔环路，极大地降低了系统的复杂性，兼具成本低的优势。在倍频器两端通过集成光纤输入输出，就可以实现倍频模块的即插即用。如图 5 所示，当基频光波长为 1018.9 nm 时，对应倍频的最佳温度 T_c 为 51.9 ℃，其半峰全宽对应的温度带宽 ΔT 为 0.9 ℃。在不同功率的基频光注入下，509 nm 激光输出功率如图 6 所示。可见，当基频光功率为 5 W 时，最大可以获得 470 mW 绿光输出，倍频转化效率为 9.6%。

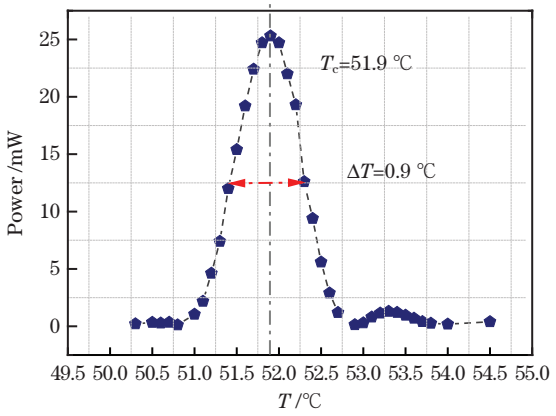

图 5 509 nm 倍频的温度匹配曲线(基频光波长为 1018.9 nm，最佳匹配温度为 51.9 ℃，半峰全宽为 0.9 ℃)

Fig. 5 Matched temperature curve of 509 nm doubled frequency system (the fundamental wavelength is 1018.9 nm, the optimal temperature is 51.9 ℃, and the full width at half maxima is 0.9 ℃)

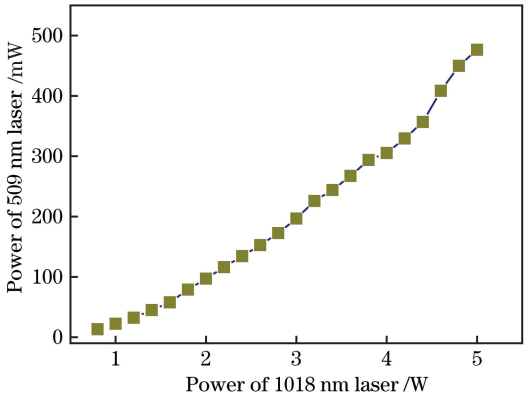

图 6 放大器注入基频光功率和倍频光输出功率之间的关系

Fig. 6 Relationship between output second-harmonic laser and injected fundmental wave powers

3 铯里德堡原子 EIT 实现

利用得到的激光系统，在热原子气室中实现了铯里德堡原子 EIT。如图 2 所示系统，852 nm 激光输出后经过二分之一波片和偏振分束棱镜，其中：反射光用于制备消多普勒效应的饱和吸收光谱(用于频率锁定)，得到的光谱如图 4 所示，将其锁定至 $6S_{1/2}|F=4\rangle\rightarrow 6P_{3/2}|F'=5\rangle$ 共振跃迁线上；透射的 852 nm 激光导入铯原子蒸气室作为里德堡原子 EIT 的探测光。将 509 nm 激光作为耦合光，采用波长计监视激光输出波长，将耦合光频率调谐至跃迁线 $6P_{3/2}|F'=5\rangle\rightarrow 67D_{5/2}$ 上。耦合光经过双色镜后与 852 nm 激光反向重合，并通过铯原子蒸气室。509 nm 光束的直径约为 800 μm，功率约为 20 mW；852 nm 激光的功率为 10 μW，光束直径约为 900 μm。调节 1018 nm 种子激光器 PZT 的偏置电压和驱动电流，将耦合光波长调谐至 508.963 nm 附近，并外加三角波于 PZT 上。由于波长线性传递效应，509 nm 耦合激光波长也会相应地进行周期性连续调谐。

852 nm 激光经过蒸气室后经过单片双色镜(509 nm 高反，852 nm 高透)，采用 9.4×10^6 V/W 的高增益光电探测器收集透射光。在探测器前加滤光片，以避免外界杂散光和室内灯光对探测器的辐照。探测光在耦合光不同失谐量处的透射强度如图 7 所示，透射增强的位置即为 EIT 信号。由于探

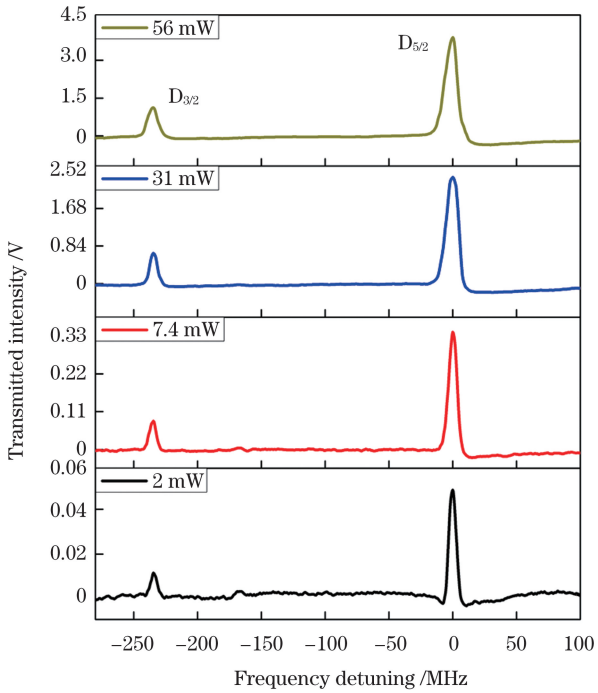

图 7 不同耦合光功率下的 EIT 信号(纵坐标为探测光的透射强度，横坐标为耦合光的失谐量)

Fig. 7 EIT signal in different coupling beam powers (vertical axes represent transmitted intensity of probe beam, horizontal axes represent frequency detuning of coupling beam)

测光共振于基态和中间激发态，只沿着光传输方向与接近零速度的群原子相互作用，因此在探测光的透射谱中无多普勒背景。探测光与耦合光的反向传输构型可以消除多普勒效应，提高光谱信噪比[35]。探测光采用相位型电光调制器（EOM）外加射频调制在原 EIT 透射峰两侧产生射频边带，以此边带和主峰间隔的频率差，将光谱的时间轴转换成激光频率。由图 7 可以看出：零失谐位置是 $D_{5/2}$ 态对应的 EIT 透射峰；负失谐 248 MHz 处是 $D_{3/2}$ 态对应的 EIT 信号，该信号较弱（这是由于 $6P_{3/2}|F'=5\rangle\rightarrow 67D_{3/2}$ 的耦合跃迁强度较小）。改变耦合光功率，得到图 7 所示 4 组不同耦合光功率下的 EIT 谱，通过比较光谱峰值可以看出耦合光功率越大，EIT 的峰值越高。

4 结 论

对于阶梯型 EIT，随着耦合光功率增大，中间态和里德堡态的耦合增强，抑制了中间激发态的原子数布局，使得里德堡态和基态的相干叠加态信号的幅值显著增大，因此增大了 EIT 的峰值。这种方式对原子谱线展宽机制的影响较小。EIT 峰值会随着探测光功率增加而有相应的增加，但谱峰的半峰全宽也会相应增加，这主要源于强探测光导致的功率展宽机制。在小场强测量情况下，应尽可能地提供足够大的耦合光功率，以提升 EIT 谱线的信号背景比，增强探测灵敏度。同时，在大的微波电场强度下，EIT 谱线在分裂的同时会有一定展宽，导致光谱峰值降低，信噪比较小，寻峰不准确。本系统可以在较大场强下使分裂间隔变大，同时使分裂光谱峰值足够高，从而保证了电场强度幅值测量的动态范围较大。

本文提出了一种工程适用性强、稳定性高的里德堡原子激发光系统方案。探测光由猫眼式半导体激光器发出，激光线宽可以保持为几十千赫兹，而且波长调谐灵活，兼顾了快速反馈和慢速反馈通道的锁频方式。耦合光采用单频窄线宽的 509 nm 激光，其实现方式为：经光纤放大器后再通过单通晶体倍频。耦合光的输出功率约为 500 mW，其输出功率和线宽质量可满足铯原子里德堡态制备和 EIT 信号的优化测量实验，为下一步搭建可靠的基于原子气室的微波场强测量系统奠定了基础。

参 考 文 献

[1] Kanda M. Standard antennas for electromagnetic interference measurements and methods to calibrate them[J]. IEEE Transactions on Electromagnetic Compatibility, 1994, 36(4): 261-273.

[2] Song Z F, Feng Z G, Liu X M, et al. Quantum-based determination of antenna finite range gain by using Rydberg atoms[J]. IEEE Antennas and Wireless Propagation Letters, 2017, 16: 1589-1592.

[3] Hall J L. Nobel Lecture: defining and measuring optical frequencies[J]. Reviews of Modern Physics, 2006, 78(4): 1279-1295.

[4] Savukov I M, Seltzer S J, Romalis M V, et al. Tunable atomic magnetometer for detection of radio-frequency magnetic fields[J]. Physical Review Letters, 2005, 95(6): 063004.

[5] Balabas M V, Karaulanov T, Ledbetter M P, et al. Polarized alkali-metal vapor with minute-long transverse spin-relaxation time[J]. Physical Review Letters, 2010, 105(7): 070801.

[6] Wasilewski W, Jensen K, Krauter H, et al. Quantum noise limited and entanglement-assisted magnetometry[J]. Physical Review Letters, 2010, 104: 133601.

[7] Koschorreck M, Napolitano M, Dubost B, et al. Sub-projection-noise sensitivity in broadband atomic magnetometry[J]. Physical Review Letters, 2010, 104(9): 093602.

[8] Hao L P, Xue Y M, Fan J B, et al. Precise measurement of a weak radio frequency electric field using a resonant atomic probe[J]. Chinese Physics B, 2020, 29(3): 033201.

[9] Mack M, Karlewski F, Hattermann H, et al. Measurement of absolute transition frequencies of ^{87}Rb to nS and nD Rydberg states by means of electromagnetically induced transparency[J]. Physical Review A, 2011, 83(5): 052515.

[10] Beterov I I, Ryabtsev I I, Tretyakov D B, et al. Quasiclassical calculations of blackbody-radiation-induced depopulation rates and effective lifetimes of Rydberg nS, nP, and nD alkali-metal atoms with $n\leqslant 80$[J]. Physical Review A, 2009, 80(5): 059902.

[11] Sedlacek J A, Schwettmann A, Kübler H, et al. Microwave electrometry with Rydberg atoms in a vapour cell using bright atomic resonances[J]. Nature Physics, 2012, 8(11): 819-824.

[12] Kumar S, Fan H Q, Kübler H, et al. Atom-based sensing of weak radio frequency electric fields using homodyne readout[J]. Scientific Reports, 2017, 7: 42981.

[13] Jing M Y, Hu Y, Ma J, et al. Atomic superheterodyne receiver based on microwave-dressed

Rydberg spectroscopy[J]. Nature Physics, 2020, 16(9): 911-915.

[14] Kumar S, Fan H, Kübler H, et al. Rydberg-atom based radio-frequency electrometry using frequency modulation spectroscopy in room temperature vapor cells[J]. Optics Express, 2017, 25(8): 8625-8637.

[15] Holloway C L, Gordon J A, Schwarzkopf A, et al. Sub-wavelength imaging and field mapping via electromagnetically induced transparency and Autler-Townes splitting in Rydberg atoms[J]. Applied Physics Letters, 2014, 104(24): 244102.

[16] Simons M T, Gordon J A, Holloway C L, et al. Using frequency detuning to improve the sensitivity of electric field measurements via electromagnetically induced transparency and Autler-Townes splitting in Rydberg atoms[J]. Applied Physics Letters, 2016, 108(17): 174101.

[17] Anderson D A, Paradis E, Raithel G, et al. High-resolution antenna near-field imaging and sub-THz measurements with a small atomic vapor-cell sensing element[C]//2018 11th Global Symposium on Millimeter Waves (GSMM), May 22-24, 2018, Boulder, CO, USA. New York: IEEE Press, 2018: 1-3.

[18] Anderson D A, Miller S A, Raithel G, et al. Optical measurements of strong microwave fields with Rydberg atoms in a vapor cell[J]. Physical Review Applied, 2016, 5(3): 034003.

[19] Anderson D A, Schwarzkopf A, Miller S A, et al. Two-photon microwave transitions and strong-field effects in a room-temperature Rydberg-atom gas[J]. Physical Review A, 2014, 90(4): 043419.

[20] Wang J M, Bai J D, Wang J Y, et al. Realization of a watt-level 319-nm single-frequency CW ultraviolet laser and its application in single-photon Rydberg excitation of cesium atoms[J]. Chinese Optics, 2019, 12(4): 701-718.
王军民, 白建东, 王杰英, 等. 瓦级 319 nm 单频连续紫外激光的实现及铯原子单光子 Rydberg 激发[J]. 中国光学, 2019, 12(4): 701-718.

[21] Hao L P, Xue Y M, Fan J B, et al. Precise measurement of a weak radio frequency electric field using a resonant atomic probe[J]. Chinese Physics B, 2020, 29(3): 033201.

[22] Fan J B, He Y H, Jiao Y C, et al. Nonlinear spectroscopy of three-photon excitation of cesium Rydberg atoms in vapor cell[J]. Chinese Physics B, 2021, 30(3): 034207.

[23] Avramescu A, Lermer T, Müller J, et al. True green laser diodes at 524 nm with 50 mW continuous wave output power on c-plane GaN[J]. Applied Physics Express, 2010, 3(6): 061003.

[24] Chen Y H, Lin W C, Shy J T, et al. Iodine-stabilized single-frequency green InGaN diode laser[J]. Optics Letters, 2017, 43(1): 126-129.

[25] Cheng Y J, Jin G, Liu X X, et al. Realization of laser system for precision measurement of microwave electric field using Rydberg atoms[J]. Journal of Astronautic Metrology and Measurement, 2021, 41(1): 48-52.
成永杰, 靳刚, 刘星汛, 等. 用于里德堡原子高精度微波电场测量的小型化激光系统设计与实现[J]. 宇航计测技术, 2021, 41(1): 48-52.

[26] Thompson D J, Scholten R E. Narrow linewidth tunable external cavity diode laser using wide bandwidth filter[J]. Review of Scientific Instruments, 2012, 83(2): 023107.

[27] Ruan J, Liu J, Ma J, et al. Robust external cavity diode laser system with high frequency stability for Cs atomic clock[J]. Chinese Optics Letters, 2010, 8(3): 300-302.

[28] Jiang Z J, Zhou Q, Tao Z M, et al. Diode laser using narrow bandwidth interference filter at 852 nm and its application in Faraday anomalous dispersion optical filter[J]. Chinese Physics B, 2016, 25(8): 083201.

[29] Zhang K, Bai J D, He J, et al. Influence of laser linewidth on the conversion efficiency of single-pass frequency doubling with a PPMgO∶LN crystal[J]. Acta Physica Sinica, 2016, 65(7): 074207.
张孔, 白建东, 何军, 等. 激光线宽对单次通过 PPMgO∶LN 晶体倍频效率的影响[J]. 物理学报, 2016, 65(7): 074207.

[30] Qian J P, Zhang L, Jiang H W, et al. 2 W single-frequency, low-noise 509 nm laser via single-pass frequency doubling of an ECDL-seeded Yb fiber amplifier[J]. Applied Optics, 2018, 57(29): 8733-8737.

[31] Su M Q, You Y, Quan Z, et al. 610-W continuous-wave single-mode green laser output based on highly efficient single-pass frequency doubling[J]. Chinese Journal of Lasers, 2021, 48(13): 1315002.
苏梦琪, 尤阳, 全昭, 等. 高效率单通倍频实现 610 W 连续波单模绿光输出[J]. 中国激光, 2021, 48(13): 1315002.

[32] Li G, Li S K, Wang X C, et al. High efficient generation of over 1 watt 509 nm laser beam by a ring cavity frequency doubler with periodically poled $KTiOPO_4$[J]. Applied Optics, 2016, 56(1): 55-60.

[33] Peng X L, Yang C S, Deng H Q, et al. Research progress of blue-green single-frequency laser[J]. Laser & Optoelectronics Progress, 2020, 57(7): 071606.

彭秀林, 杨昌盛, 邓华秋, 等. 蓝绿光单频激光器研究进展[J]. 激光与光电子学进展, 2020, 57(7): 071606.

[34] Wei L J, Cao J, Zhang Q M, et al. Frequency doubling of fiber laser based on narrow linewidth grating [J]. Laser & Optoelectronics Progress, 2021, 58(19): 1914010.
韦丽娟, 曹剑, 张庆茂, 等. 基于窄线宽光栅的光纤激光器倍频技术[J]. 激光与光电子学进展, 2021, 58(19): 1914010.

[35] Liu H F, Wang J, Yang B D, et al. Improvement of signal-to-noise ratio of electromagnetically-induced transparency spectra in the ladder-type cesium $6S_{1/2}$-$6P_{1/2}$-$8S_{1/2}$ atomic system [J]. Acta Optica Sinica, 2013, 33(10): 1030003.
刘慧丰, 王杰, 杨保东, 等. 铯原子 $6S_{1/2}$-$6P_{1/2}$-$8S_{1/2}$ 阶梯型系统中的电磁感应透明信噪比的提高[J]. 光学学报, 2013, 33(10): 1030003.

Generation of Laser System Using for Rydberg Atom Excitation

Jin Gang[1*], Cheng Yongjie[1], Huang Chengzu[1], Liu Xingxun[1], Qi Wanquan[1], He Jun[2,3]

[1] *Beijing Institute of Radio Metrology and Measurement, Beijing* 100039, *China*;

[2] *State Key Laboratory of Quantum Optics and Quantum Optics Devices, Institute of Opto-Electronics, Shanxi University, Taiyuan, Shanxi* 030006, *China*;

[3] *Collaborative Innovation Center of Extreme Optics of the Ministry of Education and Shanxi Province, Shanxi University, Taiyuan, Shanxi* 030006, *China*

Abstract

Objective The Rydberg atom can be a sensor exhibiting enhanced sensitivity to microwave electric fields due to the larger dipole moment. The demands for the 852 and 509 nm single-frequency narrow linewidth laser systems are huge in preparing Rydberg atom; however, the generation of 509 nm laser is still complicated or premature. Generally, a green laser near 509 nm is generated by direct emission from an external cavity diode laser (ECDL) or double-frequency from 1018 nm. The former only obtain power about tens of milliwatts, and ECDL with poor mechanical stability has difficulty realizing a wide range of wavelength tuning. The common frequency doubling method employs an external enhancement cavity to achieve high-efficiency and high-power frequency doubling. However, frequency doubling process is complex for the laser system. Therefore, we demonstrate a new robust, compact, and high-power green laser system using the cat-eye configure diode laser (CEDL) as a seed laser. A maximum power of 5 W was obtained from 1018 nm narrow linewidth doped ytterbium fiber amplifier (YDFA), second-harmonic generation (SHG) of 509 nm laser was from a fiber-coupled single pass periodically poled MgO-doped lithium-niobate (MgO:PPLN) nonlinear crystal with 470 mW output. The quantum number $n = 67$ Rydberg atom was prepared by the laser system. The linewidth of D state electromagnetically induced transparency (EIT) spectrum was about 5 MHz, indicating its significant role as a core part in a self-calibrating, SI-traceable broadband Rydberg atom-based radio-frequency electric field probe, and measurement instrument.

Methods CEDL is shown in Fig. 3, including three functionally different parts: diode emitter, narrow bandwidth filter, and collimator lens with cat-eye configuration. This 852 nm CEDL output power structure was scaled to 60 mW after polarization-maintaining (PM) fiber. Additionally, its center wavelength could be tuned by driver current, diode base temperature, and piezoactuator (PZT) attached at the output plate. The 1018 nm CEDL was made to be the seed of 1018 nm YDFA. The output of the seed was coupled by a PM fiber (PM980-XP, Nufern), splicing with the input of YDFA. The 509 nm single-frequency green laser was generated from 25 mm long MgO:PPLN crystal according to a single-pass crystal laser frequency doubler. A dichroic mirror was installed to separate the unwanted residual fundamental light and the generated green light after the crystal, which are highly transmittive and reflective at 509 and 1018 nm, respectively. We realized a three-level configuration using three levels with cesium (Cs) atoms: $6S_{1/2}$, $F = 4$; $6P_{3/2}$, $F = 5$; $67D_{5/2}$ (Fig. 1), to interact with a 2.28 GHz microwave field. The probe laser frequency was locked with a saturated absorption spectrum in Fig. 4. According to the two-step excitation method, the preparation of Rydberg Cs atoms was in the vapor cell at room temperature using the above laser system in Fig. 2. The probe and coupling laser beam counter-propagated through the room-temperature Cs cell, with minimized Doppler broadening of the transition. After absorption by Cs atoms, the power of the probe

light incident on the detector was recorded as the EIT spectrum when scanning the coupling laser frequency.

Results and Discussions To characterize the profit of the CEDL configuration, three points should be announced: 1) the mechanical structure stability; 2) powerful wavelength tuning ability, equipped with PZT for linear sweep tuning external cavity, current fast tuning, and temperature slow tuning ability of the laser wavelength; 3) the laser output direction will not be changed, even for a wide range of wavelength tuning. The temperature tuning curve of the single-pass SHG is shown in Fig. 5. The fundamental laser center wavelength was 1018.9 nm with an output power of 1 W. The fitting curve has a full width at half maximum bandwidth of $\Delta T = 0.9$ ℃ at the optimum phase-matching temperature of 51.9 ℃. The second-harmonic power and SHG efficiency were considered as functions of the fundamental power at the optimum phase-matching temperature (Fig. 6). When the fundament power reaches 5 W, the maximum SHG output power is scaled to 470 mW. The single-pass nonlinear conversion efficiency was 9.4%. Based on the ladder configuration Rydberg EIT spectrum in Fig. 1, the probe and coupling beam, the $1/e^2$ beam diameter were near 0.8 and 0.9 mm, respectively. The probe power incident to the vapor cell was about 10 μW. We compared the effect of coupling laser power on the EIT spectrum. The higher coupling beam power, the higher EIT peak intensity.

Conclusions In ladder type EIT, decreasing probe optical power and increasing coupling beam power can minimize the population of the middle state in vapor cell. This is essential for the lifetime of coherent state between Rydberg atom and ground state. Due to the broadening of the atomic spectral by increasing probe power, we set the probe power below the saturated intensity. In comparison, the EIT peak increases as the coupling laser power increases; however, the spectrum linewidth is only broadened slightly. For a high electric-field strength, we should increase the coupling laser power to distinguish AT splitting peaks. We have developed strong engineering applicability and high stability Rydberg atomic excitation light system based on CEDL. The laser linewidth is about tens of kHz, with a flexible wavelength tuning, providing fast and slow feedback channels for locking center frequency. The 1018 nm CEDL is the ideal seed laser for YDFA. Based on the fiber-coupled single-pass crystal frequency doubling, the power of the single-frequency narrow line width of 509 nm laser is about 470 mW. Meanwhile, its power and the linewidth parameter can meet the Cs atomic Rydberg atom EIT spectrum applications. The preparation and optimization of EIT signal measurement is the next step in building a reliable microwave field strength measurement system based on the above laser system.

Key words laser optics; Rydberg atoms; electromagnetically induced transparency (EIT); laser system; microwave electric field